Progress In Electromagnetics Research, Vol. 120, 403–421, 2011

FETD COMPUTATION OF THE TEMPERATURE DISTRIBUTION INDUCED INTO A HUMAN EYE BY A PULSED LASER

M. Cvetković[1,*], D. Poljak[1], and A. Peratta[2]

[1]Department of Electronics, University of Split, R. Boskovica 32, Split 21000, Croatia

[2]Wessex Institute of Technology, Ashurst, Southampton, SO40 7AA, UK

Abstract—In this paper we present the three-dimensional finite element time domain model of the human eye exposed to pulsed holmium: YAG laser radiation used in thermokeratoplasty procedure. The model is based on the Pennes' bioheat transfer equation and takes into account the focusing action of the lens. The absorption of laser energy inside the eye tissues is modeled using the Lambert-Beer's law. Model takes into account the pulse temporal profile. The maximum temperature values obtained from steady state and transient analysis are compared against those reported from other papers. Finally, sensitivity analysis of several parameters on the calculated temperature field is carried out.

1. INTRODUCTION

Laser systems have been widely implemented in various ophthalmological procedures during the last few decades [1–3], and these cover electromagnetic spectrum from ultraviolet to visible and infrared wavelengths. This increased use of lasers and widespread application of different types of eye surgeries have resulted in the need for quantitative understanding of basic interaction between laser light radiation and the human eye tissues. Light-tissue interaction results in either a transmission, reflection, scattering or absorption of the light [1, 2], of which, absorption is the most important process due to the fact that absorbed photon energy by a tissue results in a reemitted radiant energy, or in a light energy transformed into the heat [2]. This in

Received 4 August 2011, Accepted 31 August 2011, Scheduled 27 September 2011

* Corresponding author: Mario Cvetković (mcvetkov@fesb.hr).

turn increases a temperature field inside the tissue. Consequently, one of the most important tasks in laser surgical applications is to assess the temperature change in tissue subjected to the high intensity laser radiation.

The first attempts in quantifying the effects of electromagnetic radiation on the temperature elevation inside the eye were undertaken by Taflove and Brodwin [4], and Emery et al. [5], who computed the intraocular temperatures due to microwave radiation using the finite difference and the finite element method, respectively. Scott [6, 7] latter developed a 2D FEM model of the heat transfer inside human eye in order to study the cataract formation due to infrared radiation, and Lagendijk [8] used finite difference method to calculate temperatures inside human and animal eyes undergoing hyperthermia treatment.

Among many of the early efforts regarding the analysis of laser-tissue interaction was the one undertaken by Mainster [9], where the thermal response of a clear ocular media to radiation by infrared laser has been studied. Afterwards, Amara [10] developed a thermal model of the eye exposed to visible and infrared lasers using the finite elements, and Sbirlea and L'Huillier [11] modeled the 3D eye irradiated by argon laser using the same method, to name only a few respected papers.

Recently, Chua et al. [12] studied temperature distribution within the human eye subjected to laser source having used only four ocular tissues while not taking into account the complete eye geometry. On the other hand, Ng et al. [13], presented a full 3D model, but analysed only the steady state. Narasimhan et al. [14] used a 2D model for transient simulations of the human eye undergoing laser surgery.

Regarding the infrared radiation by a laser used for thermokeratoplasty, Manns et al. [15] presented the semianalytical model for corneal tissue slab, and Pustovalov et al. [16] model of the corneal tissue layers, respectively, while Podolt'sev and Zheltov [17] used the multilayered cylindrical model of the eye to study destructive effects on the cornea. Finally, Ooi et al. [18] presented the transient model using the boundary element method. Of these models, only that of Ooi et al. [18] took into account the actual geometry of the human eye.

The objective of this paper is related to the finite element time domain analysis of the transient temperature field distribution in the three-dimensional model of the human eye exposed to 2090 nm laser radiation, frequently used in L-TKP (laser-thermokeratoplasty) [19]. The model takes into account actual geometry of the human eye and a number of its corresponding tissues.

In Section 2 we first give a brief description of the human eye model and specify the parameters which need to be taken into account

when dealing with laser-eye thermal interaction. Furthermore, we set up the formulation, based on the Pennes' bioheat transfer equation [20], for which the solution by means of the finite element method is given. In Section 3 we present the steady state and transient results for the temperature distribution, and carry out sensitivity analysis of several parameters important in our model. The Section ends up with the discussion on the results obtained from our model and others, respectively, and give guidelines for the future work. Finally, in Section 4, the conclusion is given.

2. FORMULATION

2.1. Human Eye Modeling

Human eye is relatively small organ in the body, but at the same time represents an extremely complex system. This is particularly apparent when one tries to accurately model all or at least many of its comprising tissues. Average eye measures about 24 mm about pupillary axis and 23 mm in diameter [21]. We have assumed it to be of given dimensions, consisting of following eight homogeneous tissues: cornea, aqueous humour, lens, ciliary body, vitreous humour, sclera, choroid and retina. Figure 5, presented latter in Section 3, depicts the position of the respective tissues.

The extent and degree of tissue damage depend primarily on laser parameters such as wavelength, power density, exposure time, spot size and repetition rate [1], but optical and thermal tissue properties like absorption and scattering coefficients, heat capacity and thermal conductivity, also need to be taken into account. Unfortunately, these are not readily available. Figure 1, modified from [1], depicts how parameters are used when modelling thermal interaction in the laser-eye case.

Heat generation inside the tissue is determined by the laser parameters and the tissue optical properties, but also, when no

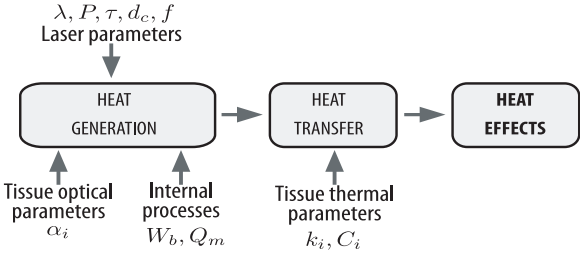

Figure 1. Parameters required for modelling. Modified from [1].

external sources are present — one needs to account for the parameters responsible for the constant temperature of the body — the volumetric perfusion rate of blood W_b and internal volumetric heat generation Q_m.

The transfer of heat to the surrounding tissues is characterised by the tissue thermal conductivity k and specific heat capacity C. Values of these parameters are given in Table 1, taken primarily from [22].

Among tissue optical properties, the most important is the absorption coefficient due to its strong dependence to the wavelength of the incident laser radiation, as can be seen in Figure 2. It follows that different eye tissues will strongly absorb only at a certain wavelengths, and will weakly absorb at the others. It is worth noting that medical lasers are based on this principle [2].

Absorption in biological tissues occurs generally due to the presence of water molecules, proteins, pigments and other macromolecules, and is governed by the Lambert-Beer's law. In the infrared region of the spectrum, high value of absorption coefficient is attributed primarily to the water molecules while in the ultraviolet and visible range, proteins and pigments are the main absorbers [1, 2, 23, 24].

Values for the absorption coefficient of the eye tissues used in the model are given in Table 1, taken from [25].

2.2. Heat Transfer in the Human Eye

The temperature distribution inside the human eye can be determined by solving the Pennes' bioheat transfer equation [20]. Pennes' equation is a non-homogeneous Helmholtz type equation that represents the

Table 1. Thermal and optical properties of various human eye tissues.

Tissue type	Volumetric perfusion rate of blood W_b	Internal heat generation Q_m	Thermal conductivity k	Specific heat capacity C	Absorption coefficient [2090 nm] α
Vitreous *h.*	0	0	0.594	3997	542.74
Lens	0	0	0.400	3000	2558.4
Aqueous *h.*	0	0	0.578	3997	2228.3
Cornea	0	0	0.580	4178	2923.8
Sclera	0	0	0.580	4178	2923.8
Cilliary body	2700	690	0.498	3340	2228.3
Choroid	0	0	0.530	3840	6398.2
Retina	35000	10000	0.565	3680	4370.4

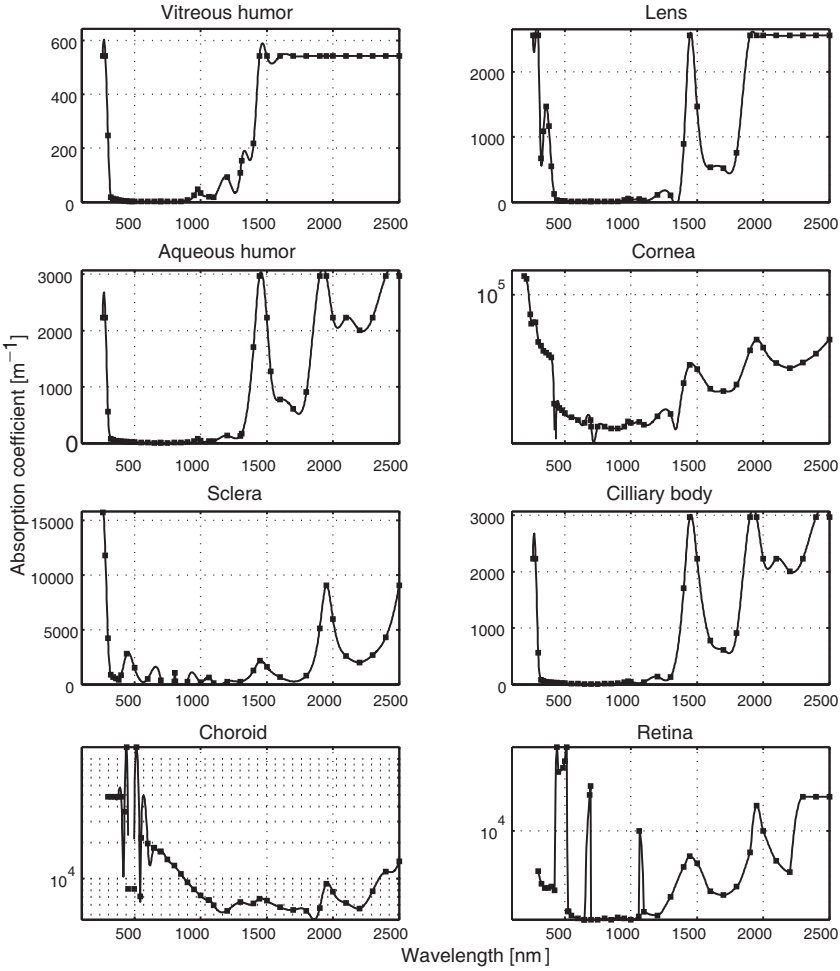

Figure 2. Absorption coefficient spectra of various human eye tissues.

energy balance between conductive heat transfer, metabolic heat generation, and heating or cooling effects due to blood perfusion:

$$\rho C \frac{\partial T}{\partial t} = \nabla \left(k \nabla T \right) + W_b C_{pb} \left(T_a - T \right) + Q_m + H \tag{1}$$

where ρ, C, W_b, C_{pb} and Q_m are, respectively, tissue density, specific heat capacity, volumetric perfusion rate, specific heat capacity of blood and internal volumetric heat generation.

The bioheat equation is extended with H — a term representing the volumetric heat generation due to external electromagnetic

irradiation [26–28]. In our model, this term is used to represent the heat generated inside the tissue due to a laser radiation.

Equation (1) is supplemented with Neumann boundary condition equations for cornea and sclera, respectively:

$$-k\frac{\partial T}{\partial n} = h_c\,(T - T_{amb}) + \sigma\epsilon\Big(T^4 - T_{amb}^4\Big) \in \Gamma_1 \tag{2}$$

$$-k\frac{\partial T}{\partial n} = h_s\,(T - T_a) \in \Gamma_2 \tag{3}$$

where k is specific tissue thermal conductivity, given in Table 1, h_c and h_s, heat transfer coefficients of cornea and sclera, respectively, σ Stefan-Boltzmann constant, ϵ emissivity of the corneal surface, T_{amb} ambient air temperature, and T_a arterial blood temperature taken to be 36.7°C. The values for h_c and h_s are taken to be $14\,\mathrm{W/m^2{}^\circ C}$ and $65\,\mathrm{W/m^2{}^\circ C}$, respectively, emissivity of the cornea is 0.975, while the value of ambient temperature is 30°C.

Equation (2) accounts for the thermal exchange between cornea and surrounding air due to convection and radiation, and in this form neglects heat loss due to evaporation, that some authors have considered in their work [13, 29]. Equation (3) represents thermal exchange between sclera and ocular globe due to convection only.

In order to avoid iterative procedure necessary when dealing with non-linear terms, such is the second term on the right hand — side of Equation (2), that represents the heat radiated to the surroundings q_{rad}, we linearize it as:

$$q_{rad} = \sigma\epsilon T_{app}^3\,(T - T_{amb}) \tag{4}$$

where T_{app}^3 is given by

$$T_{app}^3 = (T + T_{amb})\Big(T^2 + T_{amb}^2\Big) \tag{5}$$

We have approximated the value for T_{app} by segments of 10°C, taking into account different values of ambient temperature (20, 25, 30°C). Figure 3 shows plot of actual value of radiation term q_{rad} (full line) and the one calculated by using the value of T_{app} (dotted line), in the range from 20°C to 300°C.

2.3. Modeling the Laser Source

When modelling the laser source, one can use a simplifying fact that many laser beams are of a Gaussian profile. In that case, it is said that laser is operating in the fundamental transverse mode, or frequently called TEM_{00} mode of the laser. Consideration of the laser profiles other than the lowest one is beyond the scope of the present paper.

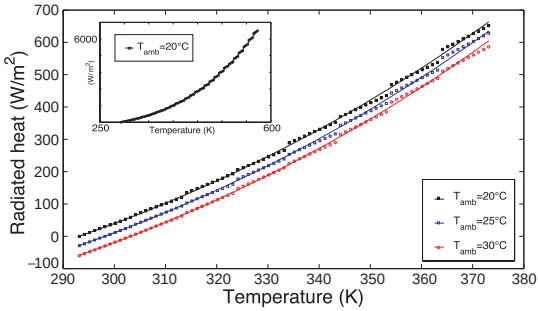

Figure 3. Approximation of a radiation term by segments of 10 K.

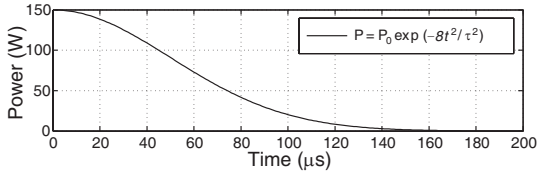

Figure 4. Laser pulse temporal profile.

This consideration is valid when the beam divergence is very small as is the case for a laser. Thus, the solutions for the electric field and the intensity can be represented in the form of a Gaussian function [1]. Interested reader can find more on the alternative approach in [30, 31], where complex representation of a laser beam is used, for the case when above approximation is not taken into account.

If we chose a cylindrical coordinates (r, z), the power density or intensity distribution at a time t is given by

$$I(r, z, t) = I_0 e^{-\alpha z} e^{-\frac{2r^2}{w^2}} e^{-\frac{8t^2}{\tau^2}} \tag{6}$$

where I_0 is the incident value of intensity, w is the beam waist, and τ is the pulse duration.

The $I_0 e^{-\alpha z}$ part represents the Lambert-Beer's law, while the last exponential term in expression (6) represents the temporal profile of a power or intensity of each laser pulse used in our model, depicted on Figure 4. The parameters used for the Ho:YAG laser where similar to those in [18] and are given latter in the results Section.

Multiplying the expression (6) with wavelength dependent absorption coefficient α of a specific tissue, i.e.,

$$H(r, z, t) = \alpha I(r, z, t) \tag{7}$$

we obtain the value for the laser energy H, absorbed by the eye tissue at the given node with cylindrical coordinates (r, z).

The pupillary opening determines a total amount of the light entering the eye [32], while image that is formed on a retina is much smaller than this aperture. If we take into account this as a focusing action of a lens, then the diameter of the image and irradiance on the retina can be calculated from

$$d_r = 2.44\frac{\lambda f}{d_p} \text{ and } I_r = I_c\frac{d_p^2}{d_r^2} \tag{8}$$

where λ is laser wavelength, f focal distance of the lens, and d_p diameter of pupillary opening. The focal distance of the lens is taken to be 17 mm [10], i.e., approximately equal to the distance from the lens to the retina.

The irradiance at the cornea is calculated for a given laser parameters from $I_c = 4P/d_c^2\pi$, where P is a laser power and d_c is a beam diameter on the cornea. The value for the beam diameter on the cornea is 0.6 mm, taken from [15].

From these values, we now interpolate the intermediate values for the beam width and irradiance along the beam path. Thus we assume that beam will propagate through all tissues along the eye pupillary axis resulting in absorption of laser energy according to absorption coefficient values of those same tissues.

It should be stressed out that this lens focusing action is the worst case scenario where all of the laser power will be concentrated onto a very small spot, while in a real situation, the eye is not such a good optical device [33], and due to this and also due to the eye movements, the image on the retina will be much larger.

2.4. Finite Element Solution

Analytical solution of (1) is limited to a few rather simple geometries with high degree of symmetry, but using the finite element method, problems on complex domains such as a human eye can be readily solved.

The steady state variant of the bioheat Equation (1) is solved first, accompanied with boundary conditions (2) and (3). The obtained results are subsequently utilized as initial conditions for the transient analysis, i.e., when the eye is subjected to laser radiation.

For the time derivative of temperature, we use $(T^i - T^{i-1})/\Delta t$, where T^i and T^{i-1} are temperatures on the nth node at current and previous time steps, respectively, while Δt represents the time step.

Multiplying Equations (1)–(3) with weight function set W_j and integrating over the entire domain Ω, we obtain the following integral

formulation

$$\int_{\Omega}\rho C\frac{\partial T}{\partial t}W_j d\Omega = \int_{\Omega}\nabla\left(k\nabla T\right)W_j d\Omega + \int_{\Omega}W_b c_b\left(T_a - T\right)W_j d\Omega + \int_{\Omega}(Q_m + H)W_j d\Omega. \quad (9)$$

Using the integration by parts, and Gauss' generalized theorem gives:

$$\int_{\Omega}\nabla\left(k\nabla T\right)W_j d\Omega = \oint_{\Gamma}k\frac{\partial T}{\partial n}W_j d\Gamma - \int_{\Omega}k\nabla T\nabla W_j d\Omega \quad (10)$$

$$\int_{\Omega}\nabla\vec{A}d\Omega = \oint_{\Gamma}\vec{A}\vec{n}d\Gamma \quad (11)$$

and the weak formulation of the Pennes' equation is obtained

$$\int_{\Omega}\rho C\frac{\partial T}{\partial t}W_j d\Omega = \oint_{\Gamma}k\frac{\partial T}{\partial n}W_j d\Gamma - \int_{\Omega}k\nabla T\nabla W_j d\Omega + \int_{\Omega}W_b c_b(T_a - T)\,W_j d\Omega + \int_{\Omega}(Q_m + H)W_j d\Omega. \quad (12)$$

Furthermore, the expressions for boundary conditions are given by

$$-\int_{\Gamma_1}k\frac{\partial T}{\partial n}W_j d\Gamma = \int_{\Gamma_1}\left(h_c + \sigma\epsilon T_{app}^3\right)TW_j d\Gamma - \int_{\Gamma_1}\left(h_c T_{amb} + \sigma\epsilon T_{app}^3 T_{amb})W_j d\Gamma \quad (13)$$

$$-\int_{\Gamma_2}k\frac{\partial T}{\partial n}W_j d\Gamma = \int_{\Gamma_2}h_s TW_j d\Gamma - \int_{\Gamma_2}h_s T_a W_j d\Gamma. \quad (14)$$

The unknown temperature distribution over an element is expressed as a linear combination of the shape functions N_j

$$T^e = \sum_{j=1}^{4}\zeta_j N_j \quad (15)$$

or in the matrix notation

$$T^e = \{N\}^T\{\zeta\} = [N_1 \quad N_2 \quad N_3 \quad N_4]\cdot\begin{bmatrix}\zeta_1\\ \zeta_2\\ \zeta_3\\ \zeta_4\end{bmatrix} \quad (16)$$

where vector $\{\zeta\}$ represents unknown coefficients of the solution.

Temperature gradient expressed in terms of shape functions can be written, as follows

$$\nabla T = \begin{bmatrix} \frac{\partial T}{\partial x} \\ \frac{\partial T}{\partial y} \\ \frac{\partial T}{\partial z} \end{bmatrix} = \begin{bmatrix} \frac{\partial N_1}{\partial x} & \frac{\partial N_2}{\partial x} & \frac{\partial N_3}{\partial x} & \frac{\partial N_4}{\partial x} \\ \frac{\partial N_1}{\partial y} & \frac{\partial N_2}{\partial y} & \frac{\partial N_3}{\partial y} & \frac{\partial N_4}{\partial y} \\ \frac{\partial N_1}{\partial z} & \frac{\partial N_2}{\partial z} & \frac{\partial N_3}{\partial z} & \frac{\partial N_4}{\partial z} \end{bmatrix} \cdot \begin{bmatrix} \zeta_1 \\ \zeta_2 \\ \zeta_3 \\ \zeta_4 \end{bmatrix} \tag{17}$$

Inserting (16) and (17) into (12) and using Galerkin-Bubnov' procedure ($W_j = N_j$), the following finite element formulation is obtained

$$\begin{aligned} &\frac{\rho C}{\Delta t}\int_\Omega T^i W_j d\Omega + \int_\Omega (k\nabla T^i \nabla W_j + W_b c_b T^i W_j) d\Omega + \\ &+ \int_{\Gamma_1} (h_c + \sigma\epsilon T_{app}^3) T^i W_j d\Gamma_1 + \int_{\Gamma_2} h_s T^i W_j d\Gamma_2 = \\ &= \int_{\Gamma_1} (h_c T_{amb} + \sigma\epsilon T_{app}^3 T_{amb}) W_j d\Gamma_1 + \int_{\Gamma_2} h_s T_a W_j d\Gamma_2 + \\ &+ \int_\Omega (W_b c_b T_a + Q_m + H) W_j d\Omega + \frac{\rho C}{\Delta t}\int_\Omega T^{i-1} W_j d\Omega \end{aligned} \tag{18}$$

Recasting the above equation into the matrix form, and solving this system using a code written in Matlab, we finally arrive to the values for the temperature T at every node in the domain, i.e., we obtain the temperature distribution inside the eye.

3. RESULTS AND DISCUSSION

We first give the results for the steady state temperature distribution in our model, which will be subsequently used as an initial conditions in the transient analysis. Also, we present the sensitivity analysis of parameters such as diameter of the pupillary opening, applied laser power, and cornea absorption coefficient, respectively, on the temperature distribution. We compare the obtained steady state and transient results of our model against those from other authors and conclude the section discussing on the results.

3.1. The Steady State Results

The steady state temperature distribution is calculated for the case when there is no laser radiation. The model has been discretized using 148,664 tetrahedral elements and 27,625 nodes. Panel a) of Figure 5 depicts the model of the human eye and associated eye

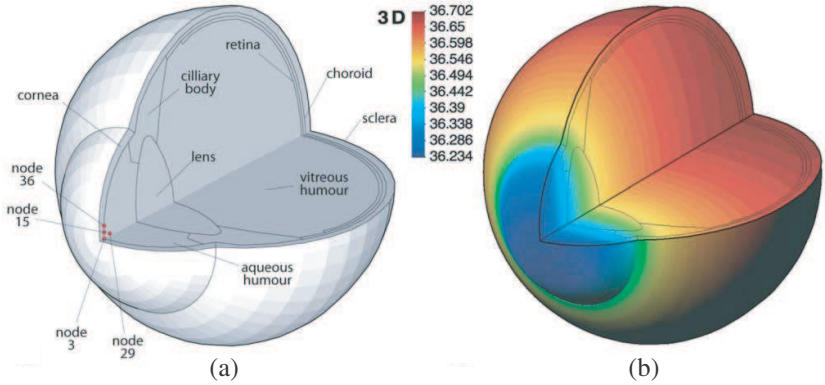

Figure 5. (a) Model of the human eye with the associated tissues. (b) The steady state temperature distribution in the eye.

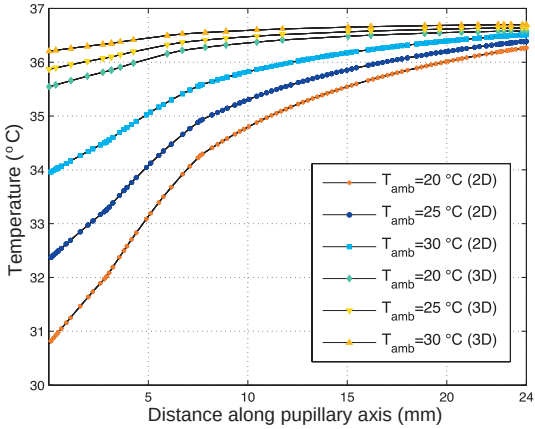

Figure 6. Steady state temperature distribution along the eye pupillary axis: Comparison against previous 2D model [34], and the dependence on the ambient temperature.

tissues, while panel b) of the same figure represents the sagittal and transverse half-plane cuts, respectively, of the steady state temperature field distribution.

Steady rise of the temperature along the eye pupillary axis can be seen on Figure 6 for three different values of ambient temperature. Also, the same figure shows temperature distribution from the anterior to the posterior parts of the eye using two-dimensional model from previous work [34]. The lower values in the anterior part of the eye

(cornea, aqueous humour) for the two-dimensional model can be clearly seen. As previously reported [35], the reason for this is the absence of the heat transfer in the direction perpendicular to the 2D model.

Various authors reported similar temperature distribution along the eye pupillary axis. The greatest temperature difference reported from those papers is at the corneal surface. Reasons for such deviations are due to a different values of ambient temperature used [6], heat transfer coefficient of cornea [6, 36, 37] or the exclusion of evaporation term in the boundary conditions [10].

Interested reader can find the summary of the steady state values of corneal surface temperatures, obtained by using a various techniques, in the work by Ng and Ooi [38]. The reported values range from 32 to 36.6°C, with the mean value at 34.66°C.

We obtained values for our three-dimensional model, ranging from 35.54°C to 36.23°C, for the ambient temperature values of 20°C and 30°C, respectively. We conclude that our steady-state results are in a good agreement with number of papers, and hence, valid.

3.2. Transient Analysis of Pulsed Ho:YAG Laser

The results from the steady state analysis will now be utilized as the initial conditions in the transient case when the eye is irradiated by the Ho:YAG 2090 nm laser. Holmium:YAG lasers are often used in the laser thermo-keratoplasty (L-TKP) vision correction procedure [19, 39]. Typical application consists of delivering several laser pulses in an annular pattern in order to induce local shrinkage of the corneal collagen.

Parameters used for this laser are: 7 pulses of 200 μs duration, laser off time between each pulse 2 sec, laser power 150 W, beam diameter on the cornea 0.6 mm, and pupil diameter 1.5 mm. Each laser pulse was sampled in ten 20 μs Δt steps, and in each of these steps, temperature distribution calculation has been carried out. For the laser cut-off period, i.e., cooling of the tissues, calculation has been done in five steps of 0.4 s Δt duration.

Figure 7 shows temperature field in the three-dimensional eye model during the application of the last laser pulse and 2 seconds after the laser has been switched off.

Figure 8 shows temperature evolution of selected nodes against calculation step (with respective distance from the cornea center). Location of these nodes is depicted on Figure 5.

Transient analysis of our model obtained significantly higher temperatures in the cornea (230.12°C — node 3) after application of seven laser pulses, compared to other authors [15, 18]. Those models reported temperatures around 110°C, and in that respect our present

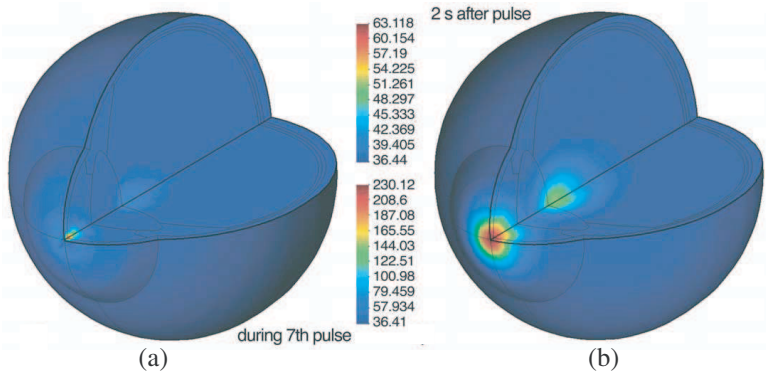

Figure 7. The temperature field distribution in the human eye; including sagittal and transverse half-plane cuts: (a) at the end of the last pulse, (b) 2 seconds after the last pulse.

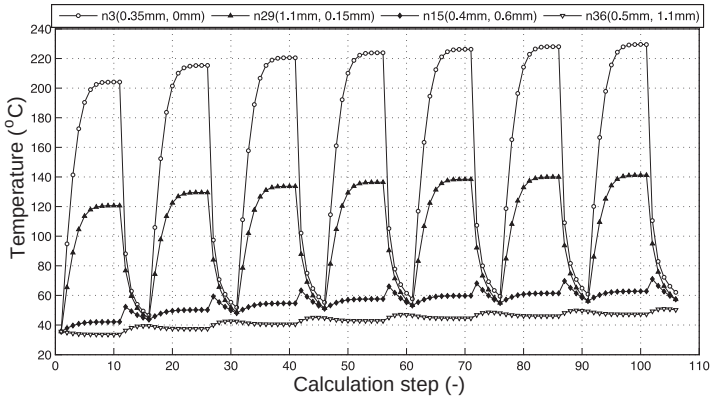

Figure 8. Temperature evolution at selected nodes. Numbers in parenthesis represent the distance from the corneal geometric center.

model overestimates the temperature. Namely, temperatures required to initiate shrinking of corneal tissues are on the order of 100°C, according to [40]. On the other hand, maximum temperatures obtained in the surrounding tissues are much lower, i.e., at node 29, located in the aqueous humour, temperature reached around 140°C. As seen from Figure 8, only the small area around the corneal site where the laser pulse has been applied is showing high value of temperature.

Since we obtained significantly higher temperatures at the cornea nodes than the respected papers, the analysis has been carried out in order to assess the importance of some of the parameters we used in the model.

Figures 9–11 show the effect of the pupillary opening, pulse power and the cornea absorption coefficient, respectively, on the maximum temperature achieved.

The analysis of the parameters showed that the diameter of the pupillary opening has a significant effect on the obtained temperature, as reported in [10, 34, 41]. In the normal human eye, the pupil diameter

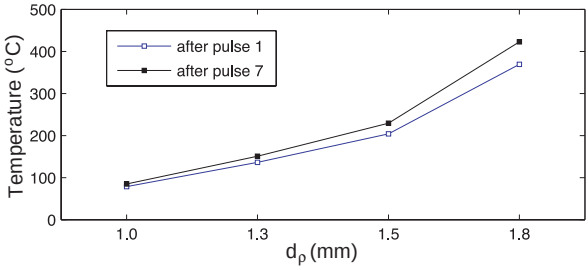

Figure 9. The effect of the pupillary opening on the maximum temperature.

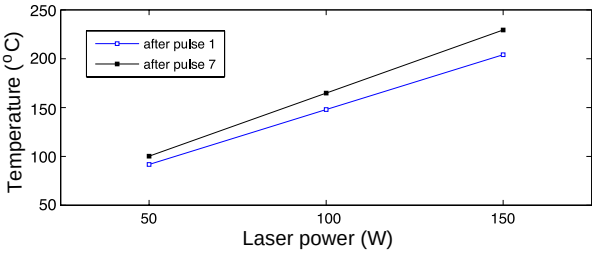

Figure 10. The effect of the applied laser power on the maximum temperature.

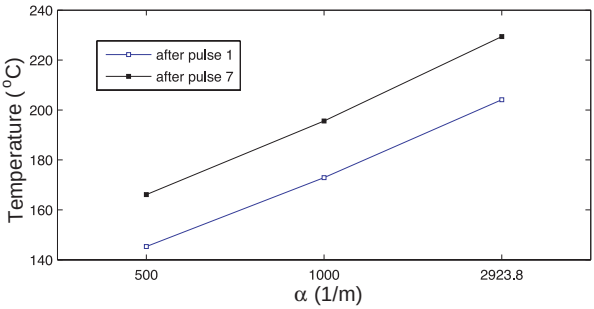

Figure 11. The effect of the absorption coefficient of cornea on the maximum temperature.

varies from 1.5 mm to about 8 mm, and is related to the ambient light conditions. It seems that the obtained temperatures, using the pupillary diameter value of 1.0 mm, much better fit the values reported by [15, 18].

Regarding the absorption coefficient value of cornea, usually, for the infrared part of the spectrum, the authors take this value to be that of the water, but it can also vary significantly. We consider here another two values along the control one of $\alpha = 2923.8\,\mathrm{m}^{-1}$, $\alpha = 500\,\mathrm{m}^{-1}$ and $\alpha = 1000\,\mathrm{m}^{-1}$. Figure 11 shows that a higher value of this parameter results in a higher temperatures achieved, i.e., greater amount of laser energy is absorbed in the corneal tissue, as was expected.

Variations of the absorption coefficient in the mid-infrared region due to increased temperature has been known [42, 43], and this dynamics has been recently taken into account in the simulation of the laser-induced thermotherapy [44]. Since we confirmed that this parameter plays significant role in the maximum temperatures achieved, values should be used with caution.

One final thing that needs to be emphasized here is related to the position of the laser beam. Using our current eye model, all seven pulses are applied to the same spot, i.e., at the center of the cornea. More elaborate way would be to take into account annular distribution of the pulses, as in [45], and thus, the lower, more physically accurate temperatures would be achieved.

4. CONCLUSION

The calculation of the steady state and transient temperature distribution inside the human eye irradiated by the Ho:YAG laser has been carried out for the three-dimensional model. In order to asses the temperature field inside the human eye during the laser radiation, we have developed a mathematical model based on the space-time dependent Pennes' bioheat transfer equation, taking into account different types of heat transfer processes. The bioheat equation has been solved using the finite elements time domain method.

In the transient analysis we have taken into account actual temporal profile of the laser pulse, along the other parameters. Although the steady state results are in an agreement with other reported results, the transient analysis obtained higher temperatures than the other respected authors, and to elucidate on this matter, parameter analysis has been carried out.

Analysis of the pupillary opening parameter showed that lower values could lead to a more acceptable results, closely matching the

temperatures reported by other authors. The analysis of the cornea absorption coefficient, that oftentimes in papers takes value from the two orders of magnitude, confirmed the importance of this parameter, and a great effort should be taken in order to obtain and validate its correct value for the specific wavelength prior to modelling of the human eye. Finally, deposition of the laser pulses in an annular manner would probably lower the temperature additionally.

As a side note, this model could be extended to predict the thermal effects to human eye tissues due to radiation by various other lasers used nowadays.

REFERENCES

1. Niemz, M. H., *Laser-Tissue Interactions: Fundamentals and Applications*, 3rd edition, Springer-Verlag, Berlin, 2003.
2. Carroll, L. and T. R. Humphreys, "LASER-tissue interactions," *Clin. in Dermatol.*, Vol. 24, 2–7, 2006.
3. Thompson, K., Q. Ren, and J. Parel, "Therapeutic and diagnostic application of lasers in ophthalmology," *Proceedings of the IEEE*, Vol. 80, No. 6, 838–860, 1992.
4. Taove, A. and M. Brodwin, "Computation of the electromagnetic fields and induced temperatures within a model of the microwave-irradiated human eye," *IEEE Trans. on Microw. and Theory*, Vol. 23, No. 11, 888–896, Jan. 1975.
5. Emery, A., P. Kramar, A. Guy, and J. Lin, "Microwave induced temperature rises in rabbit eyes in cataract research," *J. of Heat Transf.*, Vol. 97, 123–128, 1975.
6. Scott, J., "A finite element model of heat transport in the human eye," *Phys. Med. Biol.*, Vol. 33, No. 2, 227–241, 1988.
7. Scott, J., "The computation of temperature rises in the human eye induced by infrared radiation," *Phys. Med. Biol.*, Vol. 33, No. 2, 243–257, 1988.
8. Lagendijk, J., "A mathematical model to calculate temperature distributions in human and rabbit eyes during hyperthermic treatment," *Phys. Med. Biol.*, Vol. 27, No. 11, 1301–1311, 1982.
9. Mainster, M. A., "Ophthalmic applications of infrared lasers — Thermal considerations," *Invest. Ophth. Vis. Sci.*, Vol. 18, No. 4, 414–420, Apr. 1979.
10. Amara, E. H., "Numerical investigations on thermal effects of laser-ocular media interaction," *Int. J. Heat and Mass Tran.*, Vol. 38, No. 13, 2479–2488, 1995.

11. Sbirlea, G. and J. P. L'Huillier, "A powerful finite element for analysis of argon laser iridectomy: Influence of natural convection on the human eye," *WIT Tr Biomed Health*, Vol. 4, 67–79, Apr. 1997.
12. Chua, K. J., J. C. Ho, S. K. Chou, and M. R. Islam, "On the study of the temperature distribution within a human eye subjected to a laser source," *Int. Commun. in Heat and Mass Trans.*, Vol. 32, 1057–1065, 2005.
13. Ng, E. Y. K., E. H. Ooi, and U. R. Archarya, "A comparative study between the two-dimensional and three-dimensional human eye models," *Math. Comput. Model.*, Vol. 48, Nos. 5–6, 712–720, 2008.
14. Narasimhan, A., K. Jha, and L. Gopal, "Transient simulations of heat transfer in human eye undergoing laser surgery," *Int. Commun. in Heat and Mass Trans.*, Vol. 53, 482–490, Jan. 2010.
15. Manns, F., D. Borja, J. M. Parel, W. Smiddy, and W. Culbertson, "Semianalytical thermal model for subablative laser heating of homogeneous nonperfused biological tissue: Application to laser thermokeratoplasty," *J. Biomed. Opt.*, Vol. 8, No. 2, 288–297, Apr. 2003.
16. Pustovalov, V., B. Jean, T. Bende, and A. Smetannikov, "Investigations and computer modeling of the optical and thermal processes of laser thermal keratoplasty," *Laser Phys.*, Vol. 14, No. 10, 1334–1341, 2004.
17. Podol'tsev, A. and G. Zheltov, "Photodestructive effect of IR laser radiation on the cornea," *Opt. Spectrosc.*, Vol. 102, No. 1, 142–146, 2007.
18. Ooi, E. H., W. T. Ang, and E. Y. K. Ng, "A boundary element model of the human eye undergoing laser thermokeratoplasty," *Comput. Biol. Med.*, Vol. 38, 727–737, 2008.
19. Esquenazi, S., V. Bui, and O. Bibas, "Surgical correction of hyperopia," *Surv. Ophthalmol.*, Vol. 51, No. 4, 381–418, 2006.
20. Pennes, H. H., "Analysis of tissue and arterial blood temperatures in the resting human forearm, 1948," *J. Appl. Physiol.*, Vol. 85, No. 1, 5–34, Jul. 1998.
21. Smerdon, D., "Anatomy of the eye and orbit," *Curr. Anaesth. & Crit. Care*, Vol. 11, No. 6, 286–292, Jan. 2000.
22. DeMarco, S. C., G. Lazzi, W. Liu, J. D. Weiland, and M. S. Humayun, "Computed SAR and thermal elevation in a 0.25-mm 2-D model of the human eye and head in response to an implanted retinal stimulator — Part I: Models and methods,"

IEEE Transactions on Antennas and Propagation, Vol. 51, No. 9, 2274–2285, 2003.

23. Makous, W. L. and J. D. Gould, "Effects of lasers on the human eye," *IBM J. Res. and Dev.*, Vol. 12, No. 3, 257–271, 1968.
24. Krauss, J., C. Puliafito, and R. Steinert, "Laser interactions with the cornea," *Surv. Ophthalmol.*, Vol. 31, No. 1, 37–51, Jan. 1986.
25. Cvetkovic, M., A. Peratta, and D. Poljak, "Thermal modelling of the human eye exposed to infrared radiation of 1064 nm Nd:YAG and 2090 nm Ho:YAG lasers," *Wit Tr Biomed Health*, Vol. 14, 221–231, 2009.
26. Poljak, D., A. Peratta, and C. A. Brebbia, "The boundary element electromagnetic — Thermal analysis of human exposure to base station antennas radiation," *Eng. Anal. with Bound. Elem.*, Vol. 28, 763–770, Jan. 2004.
27. Ibrahiem, A., C. Dale, W. Tabbara, and J. Wiart, "Analysis of the temperature increase linked to the power induced by RF source," *Progress In Electromagnetics Research*, Vol. 52, 23–46, 2005.
28. Hirata, A., H. Sugiyama, and O. Fujiwara, "Estimation of core temperature elevation in humans and animals for whole-body averaged SAR," *Progress In Electromagnetics Research*, Vol. 99, 53–70, 2009.
29. Ooi, E., W. Ang, and E. Y. K. Ng, "A boundary element model for investigating the effects of eye tumor on the temperature distribution inside the human eye," *Comput. Biol. Med.*, Vol. 39, 667–677, Jan. 2009.
30. Mahillo-Isla, R., M. J. Gonzáles-Morales, and C. Dehesa-Martínez, "Plane wave spectrum of 2D complex beams," *Journal of Electromagnetic Waves and Applications*, Vol. 23, Nos. 8–9, 1123–1131, 2009.
31. Gonźales-Morales, M. J., R. Mahillo-Isla, E. Gago-Ribas, and C. Dehesa-Martínez, "3D complex beams in the spatial and the spectral domains," *Journal of Electromagnetic Waves and Applications*, Vol. 24, Nos. 8–9, 1103–1112, 2010.
32. Cember, H., *Introduction to Health Physics*, 3rd edition, McGraw Hill, Inc., New York, 1996.
33. Träger, F., *Springer Handbook of Lasers and Optics*, Springer Science + Business Media, LLC New York, 2007.
34. Cvetkovic, M., D. Cavka, D. Poljak, and A. Peratta, "3D FEM temperature distribution analysis of the human eye exposed to laser radiation," *Proc. Biomed.*, 2009.

35. Acharya, R. U., E. Y. K. Ng, and J. S. Suri, *Image Modeling of the Human Eye*, Chapter 11, 229–252, Artech House, Inc., 2008.
36. Ng, E. Y. K. and E. H. Ooi, "FEM simulation of the eye structure with bioheat analysis," *Comput. Meth. Prog. Bio.*, Vol. 82, 268–276, 2006.
37. Ooi, E. H., W. T. Ang, and E. Y. K. Ng, "Bioheat transfer in the human eye: A boundary element approach," *Eng. Anal. eight Bound. Elem.*, Vol. 31, No. 6, 494–500, 2007.
38. Ng, E. Y. K. and E. H. Ooi, "Ocular surface temperature: A 3D FEM prediction using bioheat equation," *Comput. Biol. Med.*, Vol. 37, 829–835, 2007.
39. Stringer, H. and J. Parr, "Shrinkage temperature of eye collagen," *Nature*, Vol. 204, No. 4965, 1307–1307, Dec. 1964.
40. Brinkmann, R., J. Kampmeier, U. Grotehusmann, A. Vogel, N. Koop, M. Asiyo-Vogel, and R. Birngruber, "Corneal collagen denaturation in laser thermokeratoplasty," *P. Soc. Photo.-Opt. Ins.*, Vol. 2681, No. 56, 56–63, Jan. 1996.
41. Cvetkovic, M., D. Poljak, and A. Peratta, "Thermal modelling of the human eye exposed to laser radiation," *Proc. SoftCOM*, Vol. 10, 16–20, 2008.
42. Jansen, E. D., T. G. van Leeuwen, M. Motamedi, C. Borst, and A. J. Welch, "Temperature dependence of the absorption coefficient of water for midinfrared laser radiation," *Laser Surg. Med.*, Vol. 14, No. 3, 258–268, 1994.
43. Lange, B., T. Brendel, and G. Hüuttmann, "Temperature dependence of light absorption in water at holmium and thulium laser wavelengths," *Appl. Optics*, Vol. 41, No. 27, 5797–5803, Sep. 2002.
44. Zhou, J., J. K. Chen, and Y. Zhang, "Simulation of laser-induced thermotherapy using a dual-reciprocity boundary element model with dynamic tissue properties," *IEEE on Trans. Bio. Eng.*, Vol. 57, No. 2, 238–245, Jan. 2010.
45. Jha, K. and A. Narasimhan, "Three-dimensional bio-heat transfer simulation of sequential and simultaneous retinal laser irradiation," *Int. J. Therm. Sci.*, Vol. 50, No. 7, 1191–1198, 2011.